Journal of The Electrochemical Society, **160** (1) G1-G5 (2013)
0013-4651/2013/160(1)/G1/5/$28.00 © The Electrochemical Society

Optoelectronic Characteristics of Organic Light-Emitting Diodes with a Rb_2CO_3-Mixed C_{60} Layer as an Electron Ohmic-Contact

Jong Tae Lim,[a] Jin Woo Park,[a] Jae Wook Kwon,[c] Geun Young Yeom,[a,z] Kyuwook Lhm,[b] and kyoung Jae Lee[b]

[a]*School of Advanced Materials Science and Engineering, Sungkyunkwan University, Suwon 440-746, Korea*
[b]*Department of Physics and Pohang Accelerator Laboratory, POSTECH, Pohang 790-784, Korea*
[c]*Product Prestige Research Laboratory, LG Production Engineering Research Center, Pyeongtaek 451-713, Korea*

A rubidium carbonate (Rb_2CO_3)-mixed fullerene (C_{60}) layer was used as the electron ohmic-contact layer and the effect of Rb_2CO_3 mixing concentration on the optoelectronic properties of organic light-emitting diodes (OLEDs) was investigated. The performance of an electron-only device, with a glass/ITO/Rb_2CO_3-mixed C_{60} (10 nm)/Al structure, was strongly dependent on both the thickness and the mixing concentration of the Rb_2CO_3 layer in the Rb_2CO_3-mixed C_{60} thin films. The ultraviolet photoemission spectra of the Rb_2CO_3-mixed fullerene (C_{60}) layer showed the formation of new Fermi level crossing states, below the Fermi level caused by a chemical interaction between Rb species and C_{60}, and which led the n-mixing effect to the contact. The emergence of new FLCSs contributed to the formation of an electron ohmic-contact between the cathode and the organic layer by increasing the number of electron carriers. The OLED device with Rb_2CO_3-mixed C_{60} as an electron ohmic contact layer, and composed of a glass/ITO/MoO_3-mixed NPB (25%, 5 nm)/NPB (63 nm)/Alq_3 (39 nm)/Rb_2CO_3-mixed C_{60} (75%, 3 nm)/Al (150 nm) structure, showed better optoelectronic properties than the OLED fabricated with C_{60} (5 nm)/LiF (1 nm) as the electron ohmic-contact layer.
 [DOI: 10.1149/2.038301jes]

Manuscript submitted July 9, 2012; revised manuscript received October 1, 2012. Published November 6, 2012.

Organic light-emitting diodes (OLEDs) are novel light sources that offer attractive applications for flat-panel displays, flexible displays, and general-purpose lighting.[1] For various applications, OLEDs have recently received considerable attention due to their rapidly improving efficiency and performance.[2] The efficiency of OLEDs is extremely dependent on the carrier-injecting ability, which is related to the formation of resistance-free or ohmic contacts at the metal-organic interfaces. This carrier-injecting probability is strongly influenced by both the injecting barrier heights[3] and the number of carriers[4] in the thin film. Here, the injecting barrier height is defined in terms of an energy difference between the Fermi levels (E_F) of the electrodes and the relevant levels for conduction in the OLED.[5,6] Therefore, appropriate aligning of the relevant levels in organic (or inorganic)-metal contact is necessary to maximize the luminous efficiency and minimize the power consumption by developing a low-voltage carrier-injecting layer.[7]

OLEDs contain almost no intrinsic charge carriers due to their weak intermolecular coupling. In order to enhance the performance of OLEDs, the extrinsic carrier concentration needs to be increased by mixing. Strong electron acceptor and donor materials have commonly been adopted as dopants in organic hole-transporting layers (HTLs) and electron-transporting layer (ETLs) in OLEDs.[4–15] Mixing these materials into HTLs and ETLs causes a charge transfer between the host and dopant materials, which markedly increases the free carrier concentration in these mixed layers and promotes the formation of an ohmic contact at electrode-organic interfaces.[10,11]

The recent reports of several materials that yield extremely low-voltage devices has excited renewed interest in developing the next generation of contacting electrodes.[15] As a p-type dopant, transition-metal oxides such as molybdenum oxides (MoO_3)[4,6–8,14,17] tungsten oxides (WO_3),[12] vanadium oxides (V_2O_5),[13] and ReO_3[16] are promising candidates to replace the previous generation of organic hole injection layers at the anode, due to their stability and their high work function (WF). Among these p-type carrier-injecting layers, MoO_3 is frequently used as a hole-injecting layer (HIL) between a tin-doped indium oxide (ITO) layer and an HTL.[4,6–8,14,17]

As the n-type dopant, Feng et al. first reported that fullerene (C_{60}) acts as a highly conductive electron-injecting layer (EIL), forming an electron ohmic contact with a lithium fluoride (LiF)/Al bi-layer cathode.[18–20] Recently, alkali-metal carbonates such as rubidium carbonate (Rb_2CO_3)[21–23] and cesium carbonate (Cs_2CO_3)[24] have been introduced as additional n-type ohmic dopants. In the n-mixing system of Rb_2CO_3-mixed 4,7-diphenyl-1,10-phenanthroline (Bphen), ultraviolet and X-ray photoemission spectroscopy (UPS and XPS) showed that n-type mixing effects, which are an electron charge transfer from Rb_2CO_3 to Bphen and the metal-induced gap states (MIGSs) created by aluminum (Al) deposition, are both keys to the improved carrier injection efficiency.[21] Here, the MIGSs are roughly free-electron-like, are defined as a metal WF penetrating into the organic semiconductor side, and are observed at the forbidden gap between the highest occupied molecular orbital (HOMO) and the E_F.

It has been reported that alkali-metal mixing into C_{60} can be used to fabricate either a conductor or a superconductor.[25] Also, Rb_2CO_3 has been demonstrated to be a robust cathode mixing material capable of forming an interface that is stable both in air and at a device driving temperature.[21–23,26] Therefore, in this study, in order to explore a new robust electron-ohmic contact to the cathode, Rb_2CO_3-mixed C_{60} is introduced as an electron ohmic-contact layer to improve the driving performance of the OLEDs. The n-mixing effect of the Rb_2CO_3-mixed C_{60} layer at various mixing concentrations and thicknesses was investigated according to the ohmic property in the electron-only device, the electronic structure around the E_F, and the morphological property. Finally, we discuss the correlation between the device performance of OLEDs with this electron-ohmic layer and the n-mixing effects.

Experimental

The structure of the all-carrier ohmic-contact OLEDs is glass/ITO (about 10 Ω/square, Geomatec Co. Ltd.) /MoO_3, 25%)-mixed N, N'-diphenyl-N, N'-bis(1-naphthyl)-1,1'-biphenyl-4,4'-diamine (NPB, 5 nm)/NPB (63 nm)/tris(8-quinolinolato)aluminum (III) (Alq_3, 42-x nm)/[Rb_2CO_3-mixed C_{60} (y%, x = 3 nm) or C_{60} (x = 5 nm)/lithium fluoride (LiF, 1 nm)]/Al (150 nm). MoO_3-doped NPB was used as a hole-injecting layer (HIL), NPB as a HTL, Alq_3 as both a green emissive layer and an ETL, Rb_2CO_3-mixed C_{60} or C_{60}/LiF as an EIL, and aluminum (Al) as the cathode layer. Each layer was sequentially vacuum-deposited by using a thermal evaporator system. The MoO_3 and Rb_2CO_3 materials were co-evaporated with NPB and C_{60}, respectively. The fabricated devices were encapsulated by depositing a bead of epoxy around the edge of the substrate, sticking another piece of glass on the bead, and curing the epoxy in a dry nitrogen box. The emissive active area of the devices was 2.0 × 2.0 mm^2.

The electron-only device was separately fabricated with the structure of glass/ITO/Rb_2CO_3-mixed C_{60} (y%, z nm)/Al (150 nm). The mixing concentration (y%) of Rb_2CO_3 was varied as from 5 to 75% and the thickness of the Rb_2CO_3-mixed C_{60} thin film was varied from 10 to 70 nm.

[z]E-mail: gyyeom@skku.edu

The current density (J)–voltage (V)-luminance (L) characteristics were measured using a source-measure unit (2400, Keithley Instrument Inc.) while the emission intensities from the OLEDs devices were measured by using the photocurrent induced on a silicon photodiode (71608, Oriel) with a picoammeter (485, Keithley Instrument Inc.).

The Rb_2CO_3-mixed NPB interfaces were examined by using UPS at the 4B1 beam line of the Pohang Accelerator Laboratory in Korea. All the measurements and depositions were performed in an ultra-high vacuum system, consisting of a main analysis chamber (approximately 5×10^{-10} Torr) and a sample preparation chamber (approximately 5×10^{-8} Torr). For the analysis, the Rb_2CO_3-mixed C_{60} (10 nm) layers with various mixing concentrations were prepared in-situ by sequential thermal evaporation on a p-type Si wafer in an ultra-high vacuum system which was connected to the beam line in vacuum. All thicknesses were determined by timed deposition calibrated using a quartz-crystal microbalance. In the UPS measurements, the He I (21.2 eV) line from an ultraviolet source was used. The photoemission onset reflecting the WF at the surface of all samples was measured by biasing the samples at −5 V. The incident photon energy was calibrated by measuring the Au 4f level of a clean Au surface. The surface roughness of the deposited thin films was observed by atomic force microscopy (AFM, SPA-300HV, SII Nano Technology Inc.).

Results and Discussion

The charge injection efficiency and interface stability can significantly affect the overall device performance and lifetime of OLEDs. Especially for a particular driving voltage, a robust interface is required with no potential barrier to carriers in order to prevent any Joule heating at the electrode interfaces.[18] In order to explore a new robust electron-ohmic contact to the cathode, a series of electron-only device with the Rb_2CO_3-mixed C_{60} was designed to obtain a resistance-free contact.

Figure 1a shows the J-V characteristics of the electron-only devices with the ITO/Rb_2CO_3-mixed C_{60}/Al structure, as a function of the Rb_2CO_3 mixing concentration at a fixed thickness of 10 nm. Compared to the electron-only device with a mixing concentration of 5% Rb_2CO_3, the devices with a mixing concentration of 10% and above exhibit perfectly linear J-V patterns that are characteristic of a true ohmic contact at both the top and bottom interfaces. The electrical conductivities of the devices with mixing concentrations of from 10% to 75% were calculated to be about 1.5×10^{-6} S/cm. However, when the Rb_2CO_3 mixing concentration was either 5% or below, the J-V curves showed non-linear relationships, which revealed that these interfaces were typically not pinned at the E_F of electrodes and were thus strongly dependent on the Rb_2CO_3 mixing concentration. Figure 1b exhibits the J-V characteristics when the thickness of the Rb_2CO_3-mixed C_{60} layer was changed at the Rb_2CO_3 mixing concentration of 75%. The results show the ohmic-contact characteristic of the electron-only device when the thickness of the Rb_2CO_3-mixed C_{60} layer was 30 nm and below. However, the bulk resistance of the Rb_2CO_3 thin films was increased at the thickness of 30 nm above. The electron ohmic-contact property of the EIL layer without the interface resistance at an optimized condition is expected to play a critical role in the operation of a diode-type device.

To understand the mechanism for an electron-injecting property near the EIL-cathode interface, the energy levels of C_{60} mixed with various Rb_2CO_3 mixing concentrations were investigated using UPS. Figure 2 shows the UPS spectra of pristine C_{60} and C_{60} mixed with various Rb_2CO_3 mixing concentrations deposited on *p*-type Si substrates. Figure 2a shows the onset of the valence band spectra, representing the WF of the surface. Initially, as the Rb_2CO_3 mixing concentration was increased to 25%, WF was slightly increased to 0.2 eV compared to that of pristine C_{60} (4.7 eV), but as the concentration was further increased above 25%, WF was significantly decreased to 1.2 eV and 2.8 eV for 75% and 100% Rb_2CO_3, respectively, compared to that of pristine C_{60}. The shifts of these WF is estimated to be relative to the

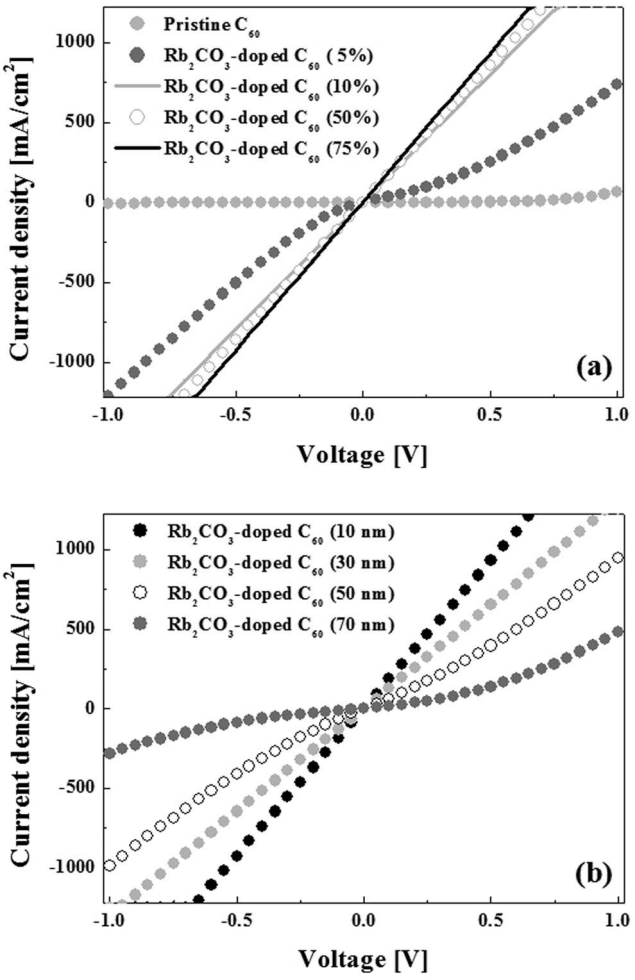

Figure 1. J-V curves of the electron-only devices which have an ITO/Rb_2CO_3-mixed C_{60}/Al structure: (a) the J-V characteristics as a function of a Rb_2CO_3 mixing concentration in the 10 nm-thick C_{60} layer, and (b) the J-V characteristics when the thickness of the Rb_2CO_3-mixed C_{60} layer was changed at the Rb_2CO_3 mixing concentration of 75%. The bias voltage was applied to the bottom electrode in reference to the top grounding electrode.

structural change when the Rb_2CO_3 mixing concentration is changed in the Rb_2CO_3-mixed C_{60} films.

Figure 2b and Fig. 2c show the valence band spectra and the region around the E_F of the Rb_2CO_3-mixed C_{60} layers, respectively. In Fig. 2b, the intensities of all curves are normalized to the incident photon flux. The bottom curve represents the photoemission spectrum for the pure C_{60}. The difference between the onsets of the HOMO level and E_F are nearly not shifted as 1.5, 1.3, 1.3, 1.5, and 1.6 eV for 0, 10, 25, 50, and 75%, respectively. The ionization energy of C_{60}, which is the sum of WF (4.7 eV) and HOMO (1.5 eV), is measured as 6.2 eV in Fig. 2b, which is consistent with a previous report.[27] Here, the energy level of the HOMO is the distance from E_F to the onset of HOMO in UPS. In addition, the C_{60} has a bandgap of about 2.5 eV.[27] In the UPS spectra of Fig. 2b, the Rb_2CO_3-mixed C_{60} film presents both HOMO-1 (at around 3.5 eV) and HOMO (at around 2.2 eV) features, which reveal higher intensities than those of pristine C_{60}. In Fig. 2c, a new Fermi level crossing state (FLCS) feature, which is aligned at the E_F such as a general metal and is partially formed by the chemical interaction between Rb species and C_{60}, starts to appear at about around 0.7 eV. The intensities of the peaks in HOMO-1, HOMO, and new FLCSs are increased as the Rb_2CO_3 mixing concentration is increased to 25%. At the mixing concentration of 50%, the intensities of HOMO-1 and HOMO features are decreased, as shown in Fig. 2b, and the width and intensity of the FLCSs in Fig. 2c grows significantly at the

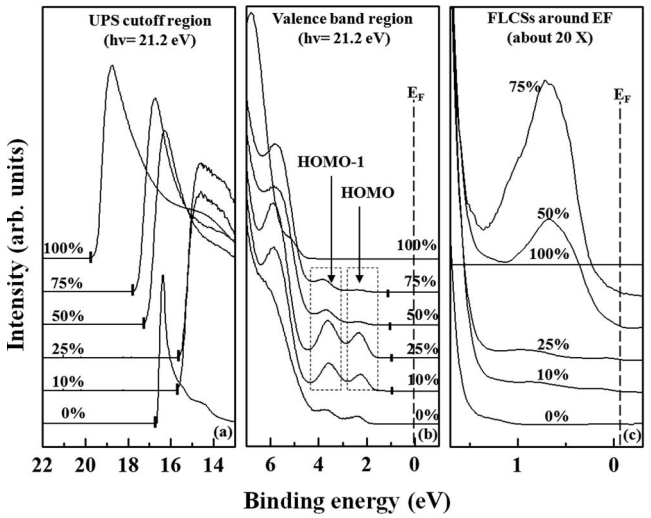

Figure 2. UPS spectra of the Rb_2CO_3-mixed C_{60} layer with various Rb_2CO_3 mixing concentrations at the fixed thickness of 10 nm: (a) the onset of the valence band, representing the WF of the surface, and (b) the valence spectra and (c) the FLCSs around the E_F of the Rb_2CO_3-mixed C_{60} layers. In (c), the region around the E_F in (b) was magnified by about 20 times. The percentages in the figures indicate the mixing concentration of Rb_2CO_3 in C_{60}. The bar indicates the onset of the WF and HOMO in Fig. 2a and Fig. 2c, respectively.

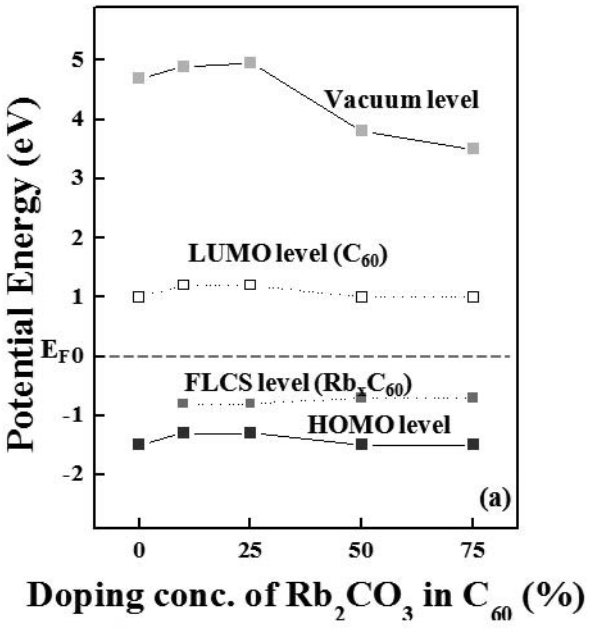

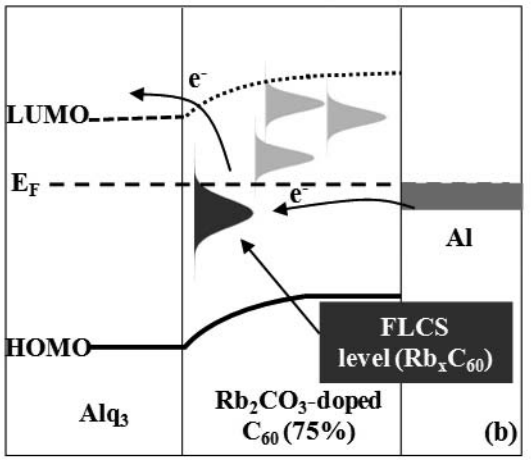

Figure 3. (a) Onset of the energy levels of the Rb_2CO_3-mixed C_{60} layer as a function of Rb_2CO_3 mixing concentration at the fixed thickness of 10 nm. WFs, FLCSs, and HOMO levels were determined by UPS. (b) Proposed energy band diagram for electron injection and electron transport at the Alq_3/Rb_2CO_3-mixed C_{60}/Al layers.

mixing concentration of 50% or higher. At the mixing concentration of 75%, the width of the FLCSs grows to about 1.3 eV, from below the E_F.

The changes of the UPS spectra on the HOMO and FLCSs are believed to be attributed to the formation of charge transfer complexes between rubidium species as an electron donor and C_{60} as an electron acceptor in the Rb_2CO_3-mixed C_{60} thin film. We suppose that the intercalation compounds of Rb_xC_{60} could be formed by two steps when Rb_2CO_3 is co-deposited with C_{60}. First, Rb_2CO_3 could be decomposed into Rb metal as a trace amount, Rb_2O_x ($1 < x$), and carbon dioxide (CO_2) during the thermal evaporation. Second, the Rb metal may be diffused into the neighboring vacant sites of C_{60}, leading to the formation of the Rb_xC_{60} intercalation compounds, as reported by other researchers.[28,29] In the case of cesium carbonate (Cs_2CO_3) deposition reported by other researchers, when Cs_2CO_3 is evaporated, almost all of the CO_2 was easily outgassed from the Cs_2CO_3 material, resulting in a formation of Cs metals or cesium oxide layers.[30]

Meanwhile, the phases, properties, and electronic structures of the Rb-intercalated C_{60} have been well characterized by several techniques.[31] Four stable phases have been reported for the Rb_xC_{60} crystal: Rb_1C_{60}, Rb_3C_{60}, Rb_4C_{60}, and Rb_6C_{60}. The intercalation of Rb atoms into C_{60} results in the formation of Rb_1C_{60} with the NaCl structure and it functions as a conductor. Rb_3C_{60} with a face-centered cubic structure is a superconductor with a relatively high critical temperature. Rb_6C_{60} is a non-conducting material with a body-centered cubic structure, and Rb_4C_{60} is a semiconductor with a body-centered tetragonal structure.[32,33]

In our experiment, the Rb-intercalated C_{60} complexes ($Rb_{1\sim3}C_{60}$) might be formed by chemical interaction during the mixing of Rb_2CO_3 to C_{60}. The increase of HOMO-1 and HOMO levels as the mixing concentration was increased to 25% could related to the formation of conducting Rb_1C_{60}, compared to the Rb-intercalated C_{60} complexes formed by the reaction between pure Rb metal and C_{60}.[28] The observed characteristic changes as the mixing concentration was increased from 10 to 25% indicated the increase of Rb_1C_{60} domains in the Rb_2CO_3-mixed C_{60} thin film. The Rb_3C_{60} phase, in which a highly conducting state (or superconductance) occurs when the triad of degenerated LUMO acquires three electrons forming a half-filled band,[34] started to form at the Rb_2CO_3 mixing concentration of 50% or higher as the spectral weight of the FLCSs at the E_F increased. The change of HOMO-1 and FLCSs intensities and the significant increase of FLCSs intensity near the E_F at the Rb_2CO_3 mixing concentration of 50% or higher are believed to be related to the formation of the Rb_3C_{60} phase. The characteristics for the Rb_xC_{60} ($x = 1 \sim 3$) formation in the UPS spectra coincided well with the synthetic mechanism of Rb-intercalated metallic Rb_3C_{60} reported by other researchers.[28,29,31]

Fig. 3 exhibits the onset of the energy levels (WF, FLCS, and HOMO) in the Rb_2CO_3-mixed C_{60} film, obtained from the results of Fig. 2. The HOMO level of the Rb_2CO_3-mixed C_{60} film was shifted within 0.2 eV, and thus did not exhibit any significant change as the mixing concentration was increased from 10 to 75%, when compared to that of the C_{60} film. On the other hand, the combined effect of the WF lowering and phase transition, and the occurrence of a new FLCSs below a E_F of 0.7 eV, due to chemical interaction between Rb species and C_{60}, not only reduced the electron injection barriers but also increased the electron concentration in the organic films, thereby explaining the improvement in the electron ohmic property, as shown in Fig. 1. These results demonstrated that Rb_2CO_3 can serve as an effective *n*-type mixant when mixed with C_{60}. In addition, the charge transfer complexes formed at the mixing concentration of 50% and

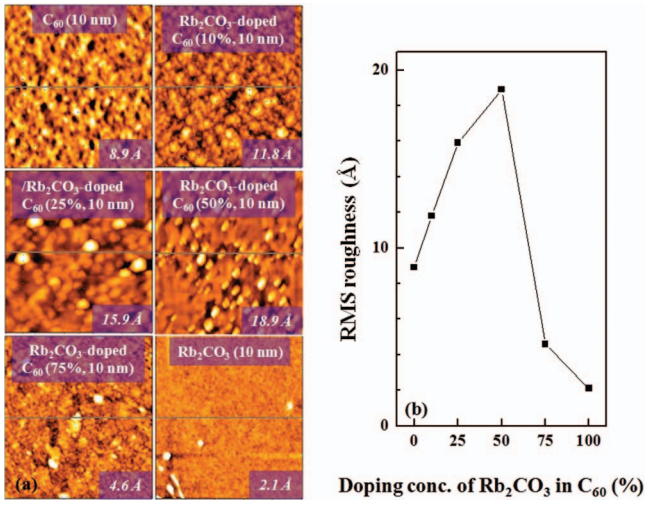

Figure 4. (a) AFM images of the surfaces of pristine C_{60} and Rb_2CO_3-mixed C_{60} (x%, x = 10, 25, 50, and 75 and pristine Rb_2CO_3 thin films) deposited on *p*-type Si wafers. (b) RMS roughness as a function of the Rb_2CO_3 mixing concentration in C_{60}. The thickness of all films was maintained at 10 nm.

higher can also improve the electron-ohmic contact property of the Rb_2CO_3-mixed C_{60} film. Figure 3b shows the proposed energy band diagram at the Alq_3/Rb_2CO_3-mixed C_{60}/Al interfaces. The electrons were efficiently injected from the E_F of Al to the FLCSs partially formed by chemical interaction between Rb species and C_{60}, which exists as a little amount in Rb_2CO_3-mixed C_{60}, and could be transported by hopping from the FCLSs of the Rb_2CO_3-mixed C_{60} layer to the LUMO level of Alq_3.

Figure 4a shows AFM images of the surfaces of pristine C_{60}, Rb_2CO_3-mixed C_{60}, and pristine C_{60} thin films deposited on *p*-Si wafer. The thicknesses of all films were maintained at 10 nm. The Rb_2CO_3 mixing concentration in the Rb_2CO_3-mixed C_{60} thin films was 0, 10, 25, 50, 75, and 100%, respectively. Figure 4b shows the change of root mean square (RMS) roughness as a function of the Rb_2CO_3 mixing concentration in C_{60}. As the mixing concentration was increased from 0 to 50%, the RMS roughness of the Rb_2CO_3-mixed C_{60} thin film was increased from 8.9 to 18.9 Å. At a mixing concentration of 75%, the RMS roughness decreased to a very smooth level of 4.6 Å. This abrupt change of RMS roughness may have been related to the phase transition occurring between the two materials from Rb_1C_{60} to Rb_3C_{60}. This smooth morphological property at a mixing concentration of 75% was expected to contribute to the stable electron-injection at the electrode-organic interface in OLEDs.

To fabricate the all-carrier ohmic OLEDs, MoO_3-doped NPB[35] was used as a hole ohmic contact and Rb_2CO_3-mixed C_{60} as the electron ohmic contact, in line with the results in Fig. 1-4. Figure 5 shows the J-V-L characteristic of OLEDs to optimize the mixing concentration of the Rb_2CO_3-mixed C_{60} layers at a fixed thickness of 3 nm. The results of Fig. 5 are summarized in Table I. The structure of Devices II∼IV was composed of glass/ITO/MoO_3-doped NPB (25%, 5 nm)/NPB (63 nm)/Alq_3 (42-x nm)/Rb_2CO_3-mixed C_{60} (y%, x = 3 nm)/Al (150 nm). The Rb_2CO_3 mixing concentrations in Devices II, III, and IV were 25, 50, and 75%, respectively. For

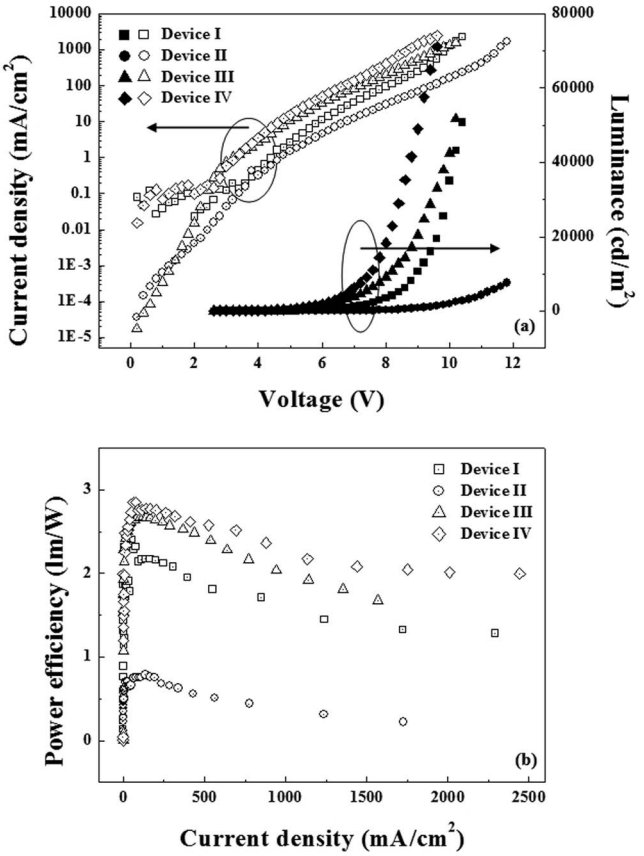

Figure 5. (a) J-V-L characteristics of OLED Devices I-IV with all-carrier ohmic-contact as a function of Rb_2CO_3 mixing concentration. The device structure is a glass/ITO/MoO_3-doped NPB (25%, 5 nm)/NPB (63 nm)/Alq_3 (42-x nm)/[Rb_2CO_3-mixed C_{60} (y%, x = 3 nm) or C_{60} (x = 5 nm)/LiF (1 nm)]/Al (150 nm). The EIL of Device I and Device II-IV consisted of C_{60}/LiF and Rb_2CO_3-mixed C_{60}, respectively. The mixing concentrations of Devices II-IV were 25, 50, and 75%, respectively. (b) Characteristics of η_{PE} vs. J for Devices I-IV.

comparison, the J-V curve of Device I, where Rb_2CO_3-mixed C_{60} as the EIL was replaced by C_{60} (x = 5 nm)/LiF (1 nm) in the same structure of the all-carrier ohmic OLEDs, is included in Fig. 5. As shown, Devices III and IV with a mixing concentration between 50 and 75% exhibited an operation voltage of 5.6 and 5.2 V at about 20 mA/cm^2, respectively. These voltages were less than the 6.6 V of Device I, used as the reference device, in which the C_{60}/LiF layer has been previously reported as a good electron ohmic-contact.[18] In contrast, Device II, with a mixing concentration of 25%, showed a higher operation voltage than Device I. Also, Devices II, III, and IV at a luminance of 1000 cd/m^2, showed a power efficiency of 0.6, 3.0, and 3.4 lm/W, respectively. Those results indicated that the EIL functioned as a good electron conductor and that the electron concentration was significantly increased at the Al/Rb_2CO_3-mixed C_{60} interface, as the mixing concentration of Rb_2CO_3 in the Rb_2CO_3-mixed C_{60} was increased from 25 to 75%. Meanwhile, the maximum luminance (L_{max}) of Devices II∼IV was 7700 (11.8 V), 51700 (10.2 V), and

Table I. J-V-L characteristics of the devices comprised of glass/ITO/MoO_3-doped NPB (25%, 5 nm)/NPB (63 nm)/Alq_3 (42-x nm)/[Rb_2CO_3-mixed C_{60} (y%, x = 3 nm) or C_{60} (x = 5 nm)/LiF (1 nm)]/Al (150 nm).

Devices	EILs	V (V) at 20 mA/cm^2	η_{PE} (lm/W) at 1000 cd/m^2	L_{max} (cd/m^2)
I	C_{60} (5 nm)/LiF (1 nm)	6.6	1.9 at 7.0 V	50800 at 10.4 V
II	Rb_2CO_3-mixed C_{60} (3 nm, 25%)	7.6	0.6 at 7.6 V	7700 at 11.8 V
III	Rb_2CO_3-mixed C_{60} (3 nm, 50%)	5.6	3.0 at 5.6 V	51700 at 10.2 V
IV	Rb_2CO_3-mixed C_{60} (3 nm, 75%)	5.2	3.4 at 5.2 V	71100 at 9.6 V

71100 cd/m^2 (9.6 V), respectively. Clearly, at a given light-emitting property, Device IV had the lowest driving voltage among the Devices investigated. The driving voltage decreased monotonically as the mixing concentration was increased, indicating that the bulk resistance of the Rb_2CO_3-mixed C_{60} layer was reduced due to the electrical n-mixing effect, which in turn reduced the hopping activation energy during the electron-injecting process in OLED. This result was in agreement with the n-mixing effect of Rb_2CO_3-mixed C_{60} shown in Figs. 1–4.

Conclusions

The mixing of Rb_2CO_3 in the C_{60} layer induced the partial formation of new complexes in the Rb_2CO_3-mixed C_{60}. Due to the chemical interaction between Rb species and C_{60}, a new FLCSs was formed below the E_F, as revealed by the UPS spectra. The generation of the new FLCSs markedly decreased the resistance contact and increased the electron carrier number. The electron-only device showed a good electron ohmic-contact property with increasing Rb_2CO_3 mixing concentration in the C_{60} layer. The device performance of the OLEDs with this electron ohmic-contact layer was consistent with both the n-mixing effect and the RMS roughness of the films. Among the OLED devices investigated, the all-carrier ohmic-contact OLED which has a glass/ITO/MoO_3-doped NPB (25%, 5 nm)/NPB (63 nm)/Alq_3 (39 nm)/Rb_2CO_3-mixed C_{60} (75%, 3 nm)/Al (150 nm) structure, showed the highest light-emitting characteristics of η_{PL} of 3.4 lm/W at 5.2 V as a function of mixing concentration of the Rb_2CO_3-mixed C_{60} electron ohmic layer.

Acknowledgments

This work is financially supported by the Ministry of Knowledge Economy (MKE) and the Korea Institute for Advancement of Technology (KIAT) through the Workforce Development Program in Strategic Technology. Also, this work was supported by Pohang Accelerator Laboratory in Korea.

References

1. K. Leo, *Nature Photonics*, **5**, 716 (2011).
2. S. R. Forrest, *Nature*, **428**, 911 (2004).
3. H. Ishii, K. Sugiyama, E. Ito, and K. Seki, *Adv. Mater.*, **11** 605 (1999).
4. W.-J. Shin, J.-Y. Lee, J. C. Kim, T.-H. Yoon, T.-S. Kim, and O.-K. Song, *Org. Electron.*, **9**, 333 (2008).
5. J. Campbell, *J. Vac. Sci. Technol. A*, **21**, 521 (2003).
6. C.-I Wu, C.-T. Lin, G.-R. Lee, T.-Y. Cho, C.-C. Wu, and T.-W. Pi, *J. Appl. Phys.*, **105**, 33717 (2009).
7. T. Matsushima and C. Adachi, *J. Appl. Phys.*, **103**, 34501 (2008).
8. T. Matsushima, Y. Kinoshita, and H. Murata, *Appl. Phys. Lett.*, **91**, 253504 (2007).
9. X. Zhou, M. Pfeiffer, J. S. Huang, J. Biochwitz-Nimoth, D. S. Qin, A. Werner, J. Drechsel, B. Maennig, and K. Leo, *Appl. Phys. Letts.*, **81**, 922 (2002).
10. M. Pfeiffer, A. Beyer, and K. Leo, *Appl. Phys. Lett.*, **73**, 3202 (1998).
11. J. Biochwitz, T. Fritz, M. Pfeiffer, K. Leo, D. M. Alloway, P. A. Lee, and N. R. Amstrong, *Org. Electron.*, **2**, 97 (2001).
12. C.-C. Chang, M.-T. Hsieh, J.-F. Chen, S.-W. Hwang, and C.-H. Chen, *Appl. Phys. Lett.*, **89**, 253504 (2006).
13. X. L. Zhu, J. X. Sun, H. J. Peng, Z. G. Meng, M. Wong, and H. S. Kwok, *Appl. Phys. Lett.*, **87**, 153508 (2005).
14. G. Xie, Y. Meng, F. Wu, C. Tao, D. Zhang, M. Liu, Q. Xue, W. Chen, and Y. Zhao, *Appl. Phys. Lett.*, **92**, 93305 (2008).
15. Z. B. Wang, M. G. Helander, M. T. Greiner, J. Qiu, and Z. H. Lu, *Phys. Rev. B*, **80**, 235325 (2009).
16. D.-S. Leem, H.-D. Park, J.-W. Kang, J.-H. Lee, J. W. Kim, and J.-J. Kim, *Appl. Phys. Lett.*, **91**, 11113 (2007).
17. T. Matsushima, G.-H. Jin, and H. Murata, *J. Appl. Phys.*, **104**, 54501 (2008).
18. X. D. Feng, C. J. Huang, V. Lui, R. S. Khangura, and Z. H. Lu, *Appl. Phys. Lett.*, **86**, 143511 (2005).
19. Y. Q. Zhao, C. J. Huang, T. Ogundimu, and Z. H. Lu, *Appl. Phys. Lett.*, **91**, 103109 (2007).
20. M. G. Helander, Z. B. Wang, and Z. H. Lu, *Appl. Phys. Lett.*, **93**, 83311 (2008).
21. M.-H. Chen, Y.-H. Chen, C.-T. Lin, G.-R. Lee, C.-I Wu, S.-S. Leem, J.-J. Kim, and T.-W. Pi, *J. Appl. Phys.*, **105**, 113714 (2009).
22. D.-S. Leem, S.-Y. Kim, J.-J. Kim, M.-H. Chen, and C.-I Wu, *Electochem. Solid St.*, **12**, J8 (2009).
23. D.-S. Leem, J.-H. Lee, J.-J. Kim, and J.-W. Kang, *Appl. Phys. Lett.*, **93**, 103304 (2008).
24. C.-I. Wu, C.-T. Lin, Y.-H. Chen, M.-H. Chen, Y.-J. Lu, and C.-C. Wu, *Appl. Phys. Lett.*, **88**, 152104 (2006).
25. O. Gunnerson, *Rev. Mod. Phys.*, **69**, 575 (1997).
26. Z. H. Lu, C. C. Lo, C. J. Huang, and Y. Y. Yuan, *Phys. Rev. B*, **72**, 155440 (2005).
27. A. Opitz, M. Bronner, and W. Brütting, *Appl. Phys. Lett.*, **90**, 212112 (2007).
28. H. Li, I. Kurash, F. Liu, and Y. Xu, *Surf. Sci.*, **540**, L631 (2003).
29. H.-N. Li, T.-Q. Wu, X. Chen, H.-Y. Li, S.-N. Bao, Y.-B. Xu, H.-J. Qian, K. Ibrahim, and F.-Q. Liu, *Chin. Phys. Lett.*, **19**, 839 (2002).
30. J. S. Yang, D. C. Choo, T. W. Kim, Y. Y. Jin, J. H. Seo, and Y. K. Kim, *Thin Solid Films*, **518**, 6149 (2010).
31. J. X. Wu, X. M. Liu, M. S. Ma, M. Bai, M. R. Ji, and J. S. Zhu, *Appl. Surf. Sci.*, **153**, 150 (2000).
32. R. M. Fleming, M. J. Rosseinsky, A. P. Ramirez, D. W. Murphy, J. C. Tully, R. C. Haddon, T. Siegrist, R. Tycko, S. H. Glarum, P. Marsh, G. Dabbagh, S. M. Zahurak, A. V. Makhija, and C. Hampton, *Nature*, **352**, 701 (1991).
33. D. M. Poler, T. R. Ohno, G. H. Kroll, P. J. Benning, F. Stepniak, J. H. Weaver, L. P. F. Chibante, and R. E. Smalley, *Phys. Rev. B*, **47**, 9870 (1993).
34. J. Tayor, H. Guo, and J. Wang, *Phys. Rev. B*, **63**, 121104 (2001).
35. J. W. Kwon, J. T. Lim, and G. Y. Yeom, *Thin Solid Films*, **518**, 6339 (2010).